International Journal of Engineering Innovation & Research
Volume 6, Issue 1, ISSN: 2277 – 5668

Design and Comparison of Axial-Flux PM BLDC Motors for Direct Drive Electric Vehicles: Conventional or Similar Slot and Pole Combination

Seyyedmahdi Jafarishiadeh* **and Mahraz Amini**
*Corresponding author email id: smjafarishiade@gmail.com

Date of publication (dd/mm/yyyy): 10/01/2017

Abstract **— Axial-flux permanent-magnet brushless-dc (AFPMBLDC) machines with concentrated windings are very attractive choices for direct-driven applications due to their high torque-density, high efficiency, and extreme compact construction. This paper presents comparison of AFPMBLDC machines having either conventional slot and pole numbers, i.e. slot number to pole number ratio of 3 to 2; or similar slot and pole numbers. To estimate the required torque of the axial-flux motors, a simple vehicle model load is considered which includes rolling resistance, aerodynamic drag, and climbing resistance. In this research cogging torque, flux linkage, back-electromotive force (back-EMF), winding inductance, and electromagnetic torque are obtained for the two AFPMBLDC motors using high precision three-dimensional finite-element (3-D FE) method. It provides useful results to be considered in design of AFPMBLDC machines.**

Keywords **— Axial Flux Permanent Magnet BLDC, Direct Drive Electric Vehicle, Pole and Slot Combination, Concentrated Winding, YASA Topology**

I. INTRODUCTION

Recently, axial-flux PM (AFPM) machine technology is developing. Axial-flux PM machines provide high efficiency, compact construction, and high torque at low speed [1-4]. Axial-flux PM machine has a high torque density compared with radial-flux PM machine and is an attractive choice especially when an electrical machine has to be directly mounted in to a mechanical machine. Good heat removal configuration along with similar aspect ratio makes AFPM machine particularly suitable for in-wheel direct drive electric vehicles [5]-[7]. Also they are suitable choices to be used in more electric aircrafts and direct-drive wind turbines [8-12]. In large scale, they can affect the power system harmonics, and in result can jump up some of the local marginal prices in the transmission level [13] On the other hand, they can affect the islanding detection by affecting the overall model at the time of charging [14].
AFPM machines which have fractional number of slots per pole and a concentrated non-overlapping winding have low cogging torque, short end-windings, and hence, a low copper loss, a high efficiency, and a high power density. However, lamination fabrication is more difficult for AFPM machines compared with their radial counterparts. Recently, the advent of soft magnetic composite (SMC) with high saturation flux density enabled researchers with new designs for novel AFPM machines, as an alternative to axially laminated steel cores. SMC allows genuine 3-D flux paths. The machine considered in this paper, shown in Fig. 1, is an SMC-based AFPM machine with a yokeless and segmented armature (YASA) topology which is used as a high-efficiency in-wheel electric drive for electric vehicle propulsion [15-18].

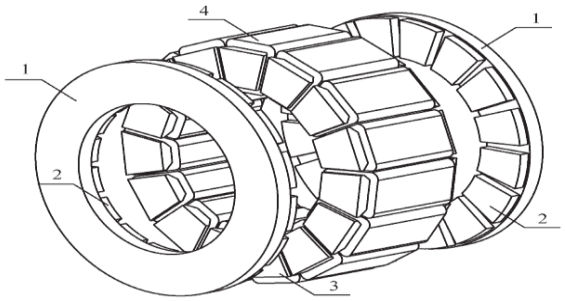

Fig. 1. Considered AFPM machine with YASA topology. (1) Rotor, (2) permanent-magnet, (3) stator segment, and (4) winding

In this paper two 3.4 kW at 1200 rpm novel AFPM machines, based on YASA topology, are designed for direct drive electric propulsion for lightweight electric vehicles. PM brushless-dc (BLDC) machines are considered for investigation in this research as they are known for high torque-density compared with PM BLAC machines [19].The investigation is carried out for two PM topologies: 15-slot/10-pole motor and 12-slot/10-pole motor. The 15-slot/10-pole machine represents conventional PM BLDC machines in which ratio of slot number to pole number is 3:2, and results in an easy winding configuration. The 12-slot/10-pole machine represents modular PM BLDC machines with similar slot number and pole number, which results in high winding factor. Cogging torque, flux linkage, back-EMF, winding inductance, and static torque are investigated for the two 3.4 kW 10-pole AFPM BLDC motors, using high precision three-dimensional finite-element analysis, which is a numerical technique for finding approximate solutions to boundary value problems for partial differential equations [120-21]. Khalili et al. developed computationally efficient elements (WSFE-based UEL) which can be used as an alternative for conventional FEM to reduce the computation time [22-23].

II. ELECTRIC VEHICLE CHARACTERISTICS

Four axial-flux motors are considered to be placed in the four vehicle wheels. To estimate the performance and approximate required torque of the axial-flux motors, a simple vehicle model load is considered. The electric

vehicle load model consists of rolling resistance (also called rolling friction or rolling drag), aerodynamic drag, and climbing resistance. The road slope and hence the climbing resistance is considered to be zero. The electric vehicle characteristics are given in Table I.

A. Aerodynamic drag

The drag force exerted on any moving object in a fluid (gas or liquid), usually appears as a depreciatory force. About 60 percent of the required power for high speed motion in vehicles is used to overcome aerodynamic drags. The aerodynamic drag on moving object (vehicle) in a fluid (air) is obtained by:

$$F_D = \frac{1}{2}\rho \upsilon^2 C_d A \tag{1}$$

B. Rolling resistance

Rolling resistance is the force resisting a motion when an object (such as a wheel, ball, etc.) is rolling on a surface. This feature is mainly created due to non-elastic characteristics, i.e. all the energy required for deformation of the wheel will not be recovered when the pressure is removed. The rolling resistance is obtained as:

$$F_r = C_{rr} N_r \tag{2}$$

where F_r is the rolling resistance, C_{rr} is the rolling resistance coefficient, and N_r is the normal force perpendicular to the surface.

The electric vehicle is considered to accelerate from 0 to 45 km/h in 9 s. So to achieve the propulsion force (F) we have:

$$F - F_r - F_D = M_c \frac{d\upsilon}{dt} \tag{3}$$

As the all-electric vehicle is expected to reach 45 km/h (=12.56 m/s) in 9 seconds, we have:

$$F - 70 - 0.177\upsilon^2 = 700\frac{d\upsilon}{dt} \Rightarrow \int_0^9 \frac{dt}{700} = \int_0^{12.56} \frac{d\upsilon}{F - 70 - 0.177\upsilon^2} \Rightarrow F = 1050N \tag{4}$$

As there are four axial-flux motors considered to be placed in the wheels, and the output radius of the axial-flux motor is 95 mm, the approximate torque of 25 Nm is required for each motor.

III. MACHINE DESIGN

To compare machine performances, machines are considered to have the same dimensions, magnetic and electric loading. The investigation is carried out for a 15-slot/10-pole AFPM motor (motor A) and a 12-slot/10-pole AFPM motor (motor B). The derivation of the sizing equation follows a similar form to the sizing equation as in [19]:

$$P = \frac{\pi^2 n p l_m \left(R_o^2 - R_i^2\right) R_i}{60\left(l_m + g'\right)} l_{bar} J K_f \alpha_s B_r \left(1 - \frac{\alpha_s l_m B_r}{\left(l_m + g'\right) B_s}\right) \tag{5}$$

where P is the output power, n is machine speed, R_o, R_i are stator outer and inner radius respectively, l_{bar} is winding axial length, J is winding current density, K_f is winding fill factor, l_m is magnet thickness and g' is effective air gap length, B_r and B_s are magnet residual flux density and maximum no load stator core flux density. The stator, magnet outer to inner diameter ratio is chosen as 0.58for maximum specific torque, in equation (5). Alarger air-gap reduces the air-gap flux density which means a larger PM is required to produce the same flux density and increases the cost. Air gap length is set to 1.5 mm due to mechanical constraints.

TABLE-1 ELECTRIC VEHICLE CHARACTERISTICS

Vehicle weight	500 kg
Passengers weight	200 kg
Full load weight (Mc)	700 kg
Frontal area	1 m2
Aerodynamic drag coefficient	0.3
Rolling resistance coefficient	0.01

Cogging torque is one of the main contributors to the torque ripple in PM motors, which is caused by the interactions between PMs and stator teeth. Pole arc to pole pitch ratio has significant effect on cogging torque. In this research cogging torque of machines are set at their minimum for different configuration. The optimum ratios of pole arc to pole pitch for minimizing cogging torque for a given slot and pole number is [24]:

$$\alpha_p = \frac{N - k_1}{N} + k_2 \quad , \qquad k_1 = 1, 2, \ldots, N - 1 \tag{6}$$

where $N=N_c/2p$, N_c is the least common multiple (LCM) between pole number ($2p$) and slot number (N_s), and $k_2$is a constant that ranges from 0.01 to 0.03 depending on air-gap length [24]. The optimum ratios of pole arc to pole pitch for minimizing cogging torque is shown in Table II. The common pole arc to pole pitch ratio of 0.7 was chosen for this study.

Slot opening is taken to be 4mm. The spacing between the stator segment shoes is expected to affect the overload capacity, and also cogging torque. Greater spacing prevents the flux leakage between the shoes and increases overload capacity, while at the same time increases cogging torque. Choosing optimum slot dimensions requires extensive considerations and analysis and is out of the scope of this research.

By neglecting the leakage flux, the total air-gap flux per pole can be calculated as the product of the flux density and area of the permanent magnet:

$$\varphi_g = B_{gap-Ave} A_{pm} = B_{gap-ave} \alpha_p \pi \frac{R_o^2 - R_i^2}{2p} \quad (7)$$

To prevent the back-iron saturation, , as shown in Figure 2, the magnetic flux density through back-iron can be expressed as:

$$\varphi_{ir} = B_{ir} A_{ir} = B_{ir} l_{ir} \left(R_o - R_i \right) \quad (8)$$

TABLE-2 OPTIMUM POLE ARC TO POLE PITCH RATIOS

15-slot/10-pole	0.36, 0.7
12-slot/10-pole	0.19, 0.36, 0.53, 0.7, 0.86

where B_{ir} is the back-iron magnetic flux density. As $\varphi_g = 2\varphi_{ir}$ and combining Eqns. (7) and (8), the back-iron length is driven by:

$$l_{ir} = \frac{B_{gap-ave}}{B_{ir}} \frac{\alpha_r \pi}{4p} \left(R_i + R_o \right) \quad (9)$$

Parallel stator slot-openings are used so that high filling factor can be achieved. When parallel slot-openings are employed, the ratio of the slot-opening width to the slot-pitch is a function of radius. The tooth widths at every radius (r) can be obtained as:

$$w = r\left({}^{2\pi}\!/_{N_s} - 2\sin^{-1}\left({}^{ds}\!/_{2r} \right) \right) \quad (10)$$

The design parameters are given in Table III. There are different ways to realize a motor with concentrated windings. It is assumed that the design is performed for three-phase motors with balanced windings which have two coils sides in each slot. The angles of the *k*th coil for the concentrated windings are defined as

$$\theta_c(k) = (k-1)\frac{2p}{N_s} 180^o E \quad (11)$$
$$for \;\; k = 1, 2, \ldots, N_s$$

where $2p$ is the number of poles and N_s is the number of slots.

With respect to (11) and for having balanced windings, the 3-phase winding arrangement is ABCABCABCABCABC for the 15-slot/10-pole machine, while it is AA′C′CBB′A′ACC′B′B for the 12-slot/10-pole machine. The winding factors K_{wn} can be achieved:

$$K_{wn} = \frac{1}{N_{cph}} \sum_{k=1}^{N_{cph}} e^{-jn\theta_c(k)} \quad (12)$$

where Ncph represents number of coils per phase, and n is the order of harmonics.

IV. SIMULATION RESULTS

Analytical methods have been used to study and predict the performance of machines, especially for initial design process or optimization of machine parameters. If saturation effects, stator and rotor slots, or exact geometric sizes are not neglected, the analytical methods will be very complex. To solve this problem and obtain results in this study for accurate comparison of two motor topologies, the finite-element method is used which applies a precise analysis of magnetic materials considering geometric details and magnetic nonlinearity. As axial-flux PM machines are inherently 3-D machines, a 3-D finite-element model was developed using software MAXWELL to study the accurate performance of the machines. To ensure results are mesh-independent, meshes were chosen small enough [25-26].

TABLE III. MOTOR PARAMETERS

Motor type	A	B
Number of poles	10	10
Number of slots	**15**	**12**
No-load Voltage , V	50	50
Rated phase current, A	34	34
Rated rotational speed, rpm	1200	1200
Stator outer radius, mm	95	95
Stator inner radius, mm	55	55
Slot-opening, mm	4	4
Tooth width at average radius, mm	27.41	35.27
pole-arc to pole-pitch ratio	0.7	0.7
Air gap, mm	1.5	1.5
Magnet axial length, mm	5	5
Magnet remanence, T	1.22	1.22
Number of turns per coil	20	25
Bar length, mm	32	32
Filling factor	0.65	0.65
Back-iron thickness, mm	10	10

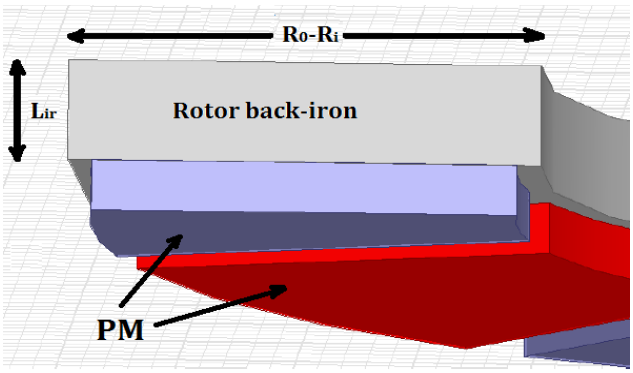

Fig. 2. Rotor back-iron thickness

Table IV shows the winding factors for the fundamental and harmonics for the two motors. It can be seen that motor B, having similar pole and slot combination, has higher fundamental winding factor which results in higher flux linkage and hence higher torque.

Torque quality of AFPM machines, which is directly related to the torque ripple components, is of high importance. Torque ripple, which is the torque pulsation caused by the periodic components in the instantaneous torque of the machine, could result in vibration, noise, and even failure [27-28]. The torque ripple of PM BLDC machine constitutes two different components, back-EMF

related torque ripple, and cogging torque which is unaffected by the load. The contribution of these components in toque ripple is investigated in following.

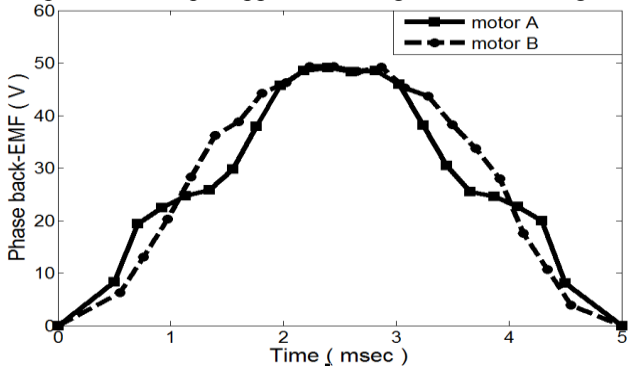

Fig. 3. Phase back-EMF waveforms by 3-D finite-element

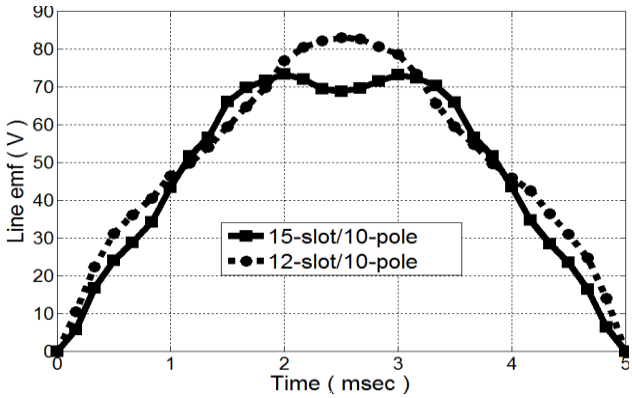

Fig. 4. Line back-EMF waveforms by 3-D finite-element

TABLE IV COMPARISON OF WINDING FACTORS

Motor Type	Harmonic order			
	n=1	*n=3*	*n=5*	*n=7*
Motor A	0.866	0	-0.866	0.866
Motor B	0.933	0.5	0.067	0.067

A. Phase back-EMF and Line back-EMF

Phase back-EMF is computed by the no-load change rate of flux linkage through the corresponding coils. Phase-back-EMF and line back-EMF waveforms of the motors are obtained and are shown in Figures 3 and 4; respectively. As in brushless-dc operation, only two phases conduct at each time, line back-EMF waveform will define the average electromagnetic torque and also back-EMF related torque ripple. It is seen in Fig. 4 that motor A has approximately flat top area, while machine B has sinusoidal top area. So machine B with similar pole number and slot number will have higher back-EMF related torque ripple.

B. Winding Inductances and Cogging Torque

Table V shows self and mutual inductances of the machines obtained by 3-D finite-element model. It is seen that machine B has higher self-inductance which can limit short circuit current better than machine A. Also machine B has lower mutual-inductance which will isolate phases from each other more effectively compared to motor A. So motor B with similar pole number and slot number provide higher fault tolerance capability. Gharghabi et al. [29-30] investigated the effect of the current harmonics and the inductance of the system parameter on the performance of the various system components.

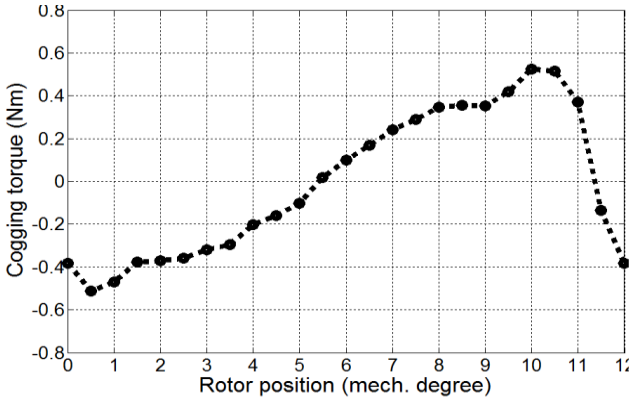

Fig.5. Cogging torque waveforms obtained for (a) motor A (b) motor B

TABLE V COMPARISON OF SELF AND MUTUAL INDUCTANCES

Motor Type	Self-inductance (mH)	Mutual inductance (mH)
Motor A	0.631	0.251
Motor B	1.21	0.106

The number of cogging torque periods per rotor revolution is equal to the LCM (least common multiple) of poles number and slots number. Higher cogging torque frequency leads to lower magnitude. It should be mentioned that for computing cogging torque waveforms having extremely low amplitude, mesh density in the finite element analysis has to be significantly high. In machine A the number of cogging torque periods per revolution is 30, while it is 60 for machine B. Cogging torque waveforms for the motors were obtained using 3-D finite-element analysis as shown in Figure 5. As can be seen in Figure 5, high cogging torque frequency reduces the level of the cogging torque. The peak to peak cogging torque of motor A is about 1 Nm for machines A with conventional pole and slot numbers, while it is about 0.2 Nm for machine B with similar pole number and slot number. So machines with similar pole number and slot number have lower cogging torque due to higher LCM.

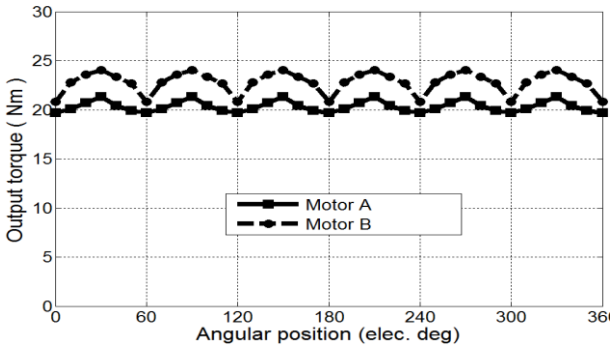

Fig. 6. Output torque waveforms by 3-D finite-element model

TABLE VI COMPARISON OF MOTOR PERFORMANCES

Motor Type	T_{max}(Nm)	T_{min}(Nm)	T_{ave}(Nm)	T_{ripple}(%)
Motor A	21.33	19.7	20.26	8.05
Motor B	24.05	20.8	22.58	14.39

C. Output Torque

Torque waveform has dominant information about motor performance including torque average and torque ripple, and the motor choice for different applications can be based on it. Machines considered in this research are supplied with 120˚ rectangular phase current waveforms (to simulate brushless-dc operation) with 34-A amplitude. The output torque was obtained as shown in Figure 6. Maximum torque, minimum torque, average torque and torque ripple of the motors are given in Table VI. It is seen that motor B with similar pole number and sloth as higher torque value due to higher winding factor, while motor A with conventional pole and slot combination has low torque ripple which makes it a good candidate for applications where low noise and vibration is important.

V. CONCLUSION

Analysis and comparison of AFPMBLDC machines having conventional slot and pole combination or similar slot and pole combination, was presented in this paper. The comparison is done for two 10-pole machines with the same PM dimension and phase current. It is shown that machines with similar slot and pole combination can better fulfill fault tolerance capability. Also machines with similar slot and pole combination have higher torque average which makes them appropriate for applications requiring high torque-density. Machines with conventional slot and pole combination have lower torque ripple which make them a good candidate where less noise and vibration is desired.

REFERENCES

[1] S. Jafarishiadeh, M. Ardebili, A. Nazari Marashi, “Investigation of pole and slot numbers in axial-flux pm bldc motors with single-layer windings for electric vehicles,” *24th Iranian Conference on Electrical Engineering (ICEE)*, 2016, pp. 1444-1448.

[2] R. Di Stefano and F. Marignetti, “Electromagnetic analysis of axial-flux permanent magnet synchronous machines with fractional windings with experimental validation”, *IEEE Trans. Ind. Electron*., vol. 59, 2012, pp. 2573-2582.

[3] K. Sitapati, R. Krishnan, “Performance comparisons of radial and axil field permanent magnet brushless machines,” *IEEE Trans. Ind. Appl*., vol. 37, no. 5, 2001, pp. 1219–1226.

[4] S. Jafari Shiadeh, M. Ardebili, and P. Moamaei, “Three-dimensional finite-element-model investigation of axial-flux PM BLDC machines with similar pole and slot combination for electric vehicles”, In: *Proceedings of Power and Energy Conference*, Illinois, 2015, pp. 1–4.

[5] J. Zhao, D. Cheng, and P. Zheng, X. Liu, C. Tong, et al. “Field weakening capability investigation of an axial flux permanent-magnet synchronous machine with radially sliding permanent magnets used for electric vehicles”, *Journal of Applied Physics*, vol. 111, no. 7, 2012, pp. 07A719 - 07A719-3.

[6] M. Babaei, M. Babaei, and M. Niasati. "Parametric analysis of overvoltages caused by back-flashover in “Siah-bishe” 400kV GIS substation." *Electric Power and Energy Conversion Systems (EPECS), 2013 3rd International Conference on. IEEE*, 2013, pp. 1-6..

[7] M. Babaei, J. Shi, N. Zohrabi, and S. Abdelwahed. "Development of a hybrid model for shipboard power systems." *In Electric Ship Technologies Symposium (ESTS)*, 2015, pp. 145-149..

[8] S. De, M. Rajne, S. Poosapati, and C. Patel, and K. Gopakumar, ‘Low-inductance axial flux BLDC motor drive for more electric aircraft,’ *IET Power Electronics*, vol. 5, no. 1, 2012, pp. 124-133.

[9] Y.S. Park, S.M. Jang, J.H. Choi, ‘Characteristic analysis on axial flux permanent magnet synchronous generator considering wind turbine characteristics according to wind speed for small-scale power application,’ *IEEE Trans. Magn*, vol. 48, no. 11, 2012, pp. 2937-2940.

[10] M. Ashkaboosi, S. M. Nourani, P. Khazaei, M. Dabbaghjamanesh, and Amirhossein Moeini. "An optimization technique based on profit of investment and market clearing in wind power systems." *American Journal of Electrical and Electronic Engineering,* vol. 4, no. 3, 2016,pp. 85-91.

[11] M. Dabbaghjamanesh, A. Moeini, M. Ashkaboosi, P. Khazaei, and K. Mirzapalangi. "High performance control of grid connected cascaded H-Bridge active rectifier based on type II-fuzzy logic controller with low frequency modulation technique." *International Journal of Electrical and Computer Engineering (IJECE)* vol. 6, no. 2, 2016, pp. 484-494.

[12] P. Khazaei, S. M. Modares, M. Dabbaghjamanesh, M. Almousa, and A. Moeini. "A high efficiency DC/DC boost converter for photovoltaic applications." *International Journal of Soft Computing and Engineering (IJSCE),* vol. 6, no. 2, 2016, pp. 2231-2307.

[13] H. Norouzi, S. Abedi, R. Jamalzadeh, M. Ghiasi Rad, S.H. Hosseinian, “Modeling and investigation of harmonic losses in optimal power flow and power system locational marginal pricing,” *Energy Journal, Science Direct,* vol. 68, 2014, pp. 140-147.

[14] H. Jouybari Moghaddam, S.H. Hosseinian, B. Vahidi, M. Ghiasi Rad, “Smart Control mode selection for propoer operation of synchronous distributed generators,” *2nd Iranian Conference on Smart Grids, Iran (Islamic Republic of)*, 2012, pp. 1-4.

[15] S. M. Jafari-Shiadeh and M. Ardebili, "Analysis and comparison of axial-flux permanent-magnet brushless-DC machines with fractional-slot concentrated-windings", *Proc. 4th Annu. Int. Power Electron., Drive Syst., Technol. Conf.*, 2013, pp. 72-77.

[16] T. J. Woolmer and M. D. McCulloch, “Analysis of the yokeless and segmented armature machine,” in *Proc. IEEE Int. Electr. Mach. Drives Conf*., vol. 1, no. 3–5, 2007, pp. 704–708.

[17] W. Fei and P. C. K. Luk, “Cogging torque reduction techniques for axialflux surface-mounted permanent-magnet segmented-armature-torus machines,” in *Proc. IEEE Int. Symp. Ind. Electr.*, 2008, pp. 485–490.

[18] H. Vansompel, P. Sergeant, L. Dupré, and A. Van den Bossche, “Axial-Flux PM Machines With Variable Air Gap,” *IEEE Trans. Ind. Electron*, vol. 61, no. 2, 2014, pp. 730-737.

[19] T.A. Lipo and F.X. Wang, “Design and performance of a converter optimized AC machines,” *IEEE Trans. on Industry Applications*, vol. IA-20, no. 4, 1984, pp. 834-844.

[20] V. Sarfi, V. Hemmati, and M. M. Arabshahi. "Simulation of PTC devices as fault current limiters in power systems by finite element

method." *In High Voltage Engineering and Application (ICHVE), 2014 International Conference on*, 2014, pp. 1-4..

[21] V. Sarfi, and V. Hemmati. "Simulation of partial discharge in closely coupled cavities embedded in solid dielectrics by finite element method." *In High Voltage Engineering and Application (ICHVE), 2014 International Conference on*, 2014, pp.1-4.

[22] A. Khalili, R. Jha, D. Samaratunga "Spectrally Formulated User-Defined Element in Conventional Finite Element Environment for Wave Motion Analysis in 2-D Composite Structures" *European Journal of Computational Mechanics*, November 11, 2016, pp. 1-29.

[23] A. Khalili, D. Samaratunga, R. Jha, T. E. Lacy, S. Gopalakrishnan "Wavelet Spectral Finite Element Based User-Defined Element in Abaqus for Modeling Delamination in Composite Beams" *23rd AIAA/ASME/AHS Adaptive Structures Conference*, Kissimmee, FL, US, 5-9 January 2015

[24] Z. Q. Zhu and D. Howe, "Improved Analytical Model for Predicting the Magnet Field Distribution in Brushless Permanent-Magnet Machines*," IEEE Tran on Magn*, vol. 38, 2002, pp. 229-238.

[25] M. Masoomi, N. Shamsaei, X. Gao, S. M. Thompson, A. Elwany, L. Bian, N. Shamsaei, L. Bian, and A. Elwany, "Modeling, simulation and experimental validation of heat transfer during selective laser melting," *in ASME 2015 International Mechanical Engineering Congress & Exposition*, 2015,pp. V02AT02A007.

[26] M. Masoomi, S. M. Thompson, N. Shamsaei, A. Elwany, and L. Bian, "An Experimental-Numerical Investigation of Heat Transfer during Selective Laser Melting," *in 26th International Solid Freeform Fabrication Symposium*, 2015, pp. 1-14.

[27] H. Saberi, M. Sabahi, M. B. B. Sharifian and M. Feyzi, "Improved sensorless direct torque control method using adaptive flux observer", *IET Power Electron*., vol. 7, no. 7, 2014, pp. 1675-1684.

[28] H. Saberi, M. B. Bannae Sharifian, M. Amiri, "Performance improvement of direct torque control drives in low speed region," *2012 2nd International eConference on Computer and Knowledge Engineering (ICCKE)*, 2012, pp. 83-88.

[29] P. Gharghabi, J. Lee, M. S. Mazzola, and T. E. Lacy., "Development of an Experimental Setup to Analyze Carbon/Epoxy Composite Subjected to Current Impulses," *Proceedings of the American Society for Composites: Thirty-First Technical Conference*, 2016.

[30] P. Gharghabi, P. Dordizadeh B., and K. Niayesh, "Impact of Metal Thickness and Field-Shaper on the Time-Variant Processes during Impulse Electromagnetic Forming in Tubular Geometries," *Journal of the Korean Physical Society*, vol. 59, no. 61, 2011, p. 3560-3566.

AUTHORS' PROFILE

Seyyedmahdi Jafarishiadeh received the B.Sc. degree in electrical engineering from Amirkabir University, Tehran, Iran, in 2010, and the M.Sc. degree in electrical engineering from K. N. Toosi University, Tehran, Iran, in 2013. His research interests are electric drives and electric machines.

Mahraz Amini received the B.Sc.and M.Sc. degree in electrical engineeringfrom University of Tehran, Tehran, Iran, in 2011 and 2014;respectively. His current research interests are power system analysis and smart grids.